Future improvements in conjunction assessment and collision avoidance using a combined laser tracking/nudging network

Heiko Dreyer [(1)], Stefan Scharring [(1)], Jens Rodmann [(1,*)], Wolfgang Riede [(2)], Christoph Bamann [(3,†)], Tim Flohrer [(2)], Srinivas Setty [(2,†)], Andrea Di Mira [(2)], Emiliano Cordelli [(2)]

[(1)] German Aerospace Centre (DLR), Institute of Technical Physics, Pfaffenwaldring 38-40, 70569 Stuttgart, Germany, corresponding author: heiko.dreyer@dlr.de
[(2)] European Space Agency – European Space Operations Centre (ESA/ESOC), Robert-Bosch-Str. 5, 64293 Darmstadt, Germany
[(3)] Technical University of Munich, Institute of Astronomical and Physical Geodesy, Arcisstraße 21, 80333 Munich, Germany

ABSTRACT

We report about the findings of our conceptual study LARAMOTIONS (SSA P3-SST-XV) funded by the European Space Agency in which simulations on laser station networks for tracking and momentum transfer have been carried out in order to analyse the possible improvements in conjunction assessment and collision avoidance in the low Earth orbit (LEO).

In this paper the software architecture for the simulations is outlined as well as the results for different network geometries considering the number of stations, their geographical distribution and local weather conditions regarding their impact on the achievable orbit accuracy. We compare on-demand tracking in response to conjunction alerts from radar-based orbital data with the operation of permanent laser tracking yielding a "laser catalogue" of debris' orbital data being independent from radar measurements. Moreover, we explore space debris nudging with photon pressure from ground-based high-power lasers in terms of a reduction of the collision rate in LEO.

1 INTRODUCTION

The expected significant increase of space launch activities in the next years, both from spacefaring nations and in the private sector, yields an enhanced risk of space debris generation. In this regard, space situational awareness (SSA) is mandatory not only for the protection of active space missions, but as a prerequisite to prevent aggravation of the space debris environment by cascading effects of secondary debris generation due to in-space collisions.

High accuracy in laser ranging to space objects (within a meter or better) has already been demonstrated, e.g., by the International Laser Ranging Service (ILRS) network. Thus, laser ranging (LR) comprising laser tracking (LT) can be considered as a highly promising sensor technology for space surveillance in the low Earth orbit which has the potential to complement existing radar facilities in terms of achievable state vector accuracy. Furthermore, several laser-based concepts on orbit modification have been proposed in the recent years [1]. In particular, momentum transfer to space debris via photon pressure appears to become feasible, due to advancements in adaptive optics and the commercial availability of high-power lasers with an average power output beyond the 10-kW level [2]. This allows for the setup of a network of comparably cost-efficient laser stations for momentum transfer (MT) in the near future paving the way for the capability to remotely operate space debris in particular in terms of debris vs. debris collision avoidance manoeuvres.

In the scope of our conceptual Laser Ranging Systems Evolution Study LARAMOTIONS funded by the European Space Agency (ESA) simulations of a ground-based laser tracking and momentum transfer (LTMT) network have been carried out in order to estimate the subsequent improvements in conjunction assessment and collision avoidance for operational satellites as well as for debris vs. debris encounters.

In this paper we report about the network simulation software architecture and the related theoretical basics together with relevant technological and astrodynamical constraints. Simulation results are shown for different network geometries considering the number of stations, their geographical distribution and local weather conditions.

As a laser ranging systems *evolution* study we start off in our analysis with the near-term laser tracking scenario based on demand arising from conjunction alerts generated from radar measurements. Departing from this scenario the evolution of such a network towards an autonomously operating SSA entity is analyzed which

---

[*] Present address: etamax space GmbH, Lilienthalplatz 1, 38108 Braunschweig, Germany
[†] Present address: Vyoma GmbH, Eckhardtstraße 28, 64289 Darmstadt, Germany

would maintain a space debris catalogue comprising orbital data generated from laser ranging exclusively.

As a different branch of network evolution from on-demand LT the establishment of laser-based momentum transfer towards an LTMT network for precise conjunction assessment including space debris maneuvers for collision avoidance will be presented in the third part of our analysis.

Finally, an outlook will be given regarding future simulations and possible enhancements of the simulation environment.

2 THEORY

For the assessment of on-demand network performance, the false alert rate (FAR) and the collision rate (CR) have been identified in the statement of work to this study as the main figures of merit. Firstly, the usage of LT systems should enable to pick relevant collision alerts. Therefore, the respective false alert rate FAR should be reduced by one order of magnitude. The FAR in conjunction alerts from radar-based measurement is defined as

$$FAR^{(Radar)} = \frac{n_{FP}^{(Radar)}}{n_{FP}^{(Radar)} + n_{TP}^{(Radar)}} \qquad (1)$$

where n_{FP} denotes the number of false positive (FP) conjunction alert and n_{TP} gives the number of true positives (TP), respectively. To assess whether an alert has to be regarded to as FP or TP, the timespan before the time of closest approach (TCA) is split into a *decision timeframe* lasting up to 48 hours before TCA and a subsequent *action timeframe* ending at TCA. If the last Conjunction Data Message (CDM) during the decision timeframe exhibits a collision probability P_c which exceeds the accepted collision probability level (ACPL) of 10^{-4}, a conjunction alert is raised which would demand for a collision avoidance manoeuvre, be it by on-board propulsion systems (for satellites) or using laser-based photon pressure (for space debris). If now the collision probability p_c at the time of the last CDM during the action timeframe still exceeds the ACPL, the respective conjunction alert is deemed true positive, otherwise FP.

The FAR of laser tracking systems, FAR_{Laser}, is computed with reference to the demand raised from radar measurements. Here, it has to be considered that a close approach event spotted by the radar system might be discarded by a laser tracking system which would constitute a false negative (FN) event in laser alerts. Hence, for the definition of FAR_{Laser} an extension has to be made using

$$FAR^{(Laser)} = \\ = \frac{n_{FP}^{(Laser)} + n_{FN}^{(Laser)}}{n_{FP}^{(Laser)} + n_{TP}^{(Laser)} + n_{FN}^{(Laser)} + n_{TN}^{(Laser)}} \qquad (2)$$

where $n_{FP}^{(Radar)} + n_{TP}^{(Radar)} = n_{FP}^{(Laser)} + n_{TP}^{(Laser)} + n_{FN}^{(Laser)} + n_{TN}^{(Laser)}$, which finally yields the following expression for the system requirement on FAR reduction:

$$\frac{n_{FP}^{(Laser)} + n_{FN}^{(Laser)}}{n_{FP}^{(Radar)}} \leq 10\ \% \qquad (3).$$

Concerning the collision rate CR as the second figure of merit, the investigated networks should aim for its reduction by 95% which has a twofold meaning. In an all-on-all conjunction analysis, CR can be defined by

$$CR = \sum_j P_{c,j} \qquad (4).$$

giving the sum over all collision probabilities of possible conjunction pairs j. CR reduction can, thus, be achieved by (1) enhancing the accuracy of orbital data by additional measurements, which reduce the related covariance, and/or (2) by modification of the trajectories themselves by a collision avoidance manoeuvre. Whereas the latter might be more intuitive, CR reduction by observation is caused by a decrease of orbit uncertainty through precise measurements, which in turn reduces the probability of collision of the corresponding close approach event [3]. Therefore, the above-mentioned system requirement on CR is analysed both for on-demand LT as well as for LTMT systems.

In contrast, FAR and CR are not reflected for the laser catalogue branch of laser ranging systems evolution. Though possible in principle, the related numerical effort would have exceeded the frame of the study. Instead, the network capacity for such a laser catalogue is analysed using analytical simplifications, cf. Sect. 4.1, in favour of a dedicated covariance propagation for space debris objects to be considered.

3 SIMULATION

For the analysis of laser tracking networks including laser-based momentum transfer operations a simulation environment has been established based on commercial software for orbit determination and propagation from Analytical Graphics, Inc. (AGI). The simulation environment makes use of AGI's Systems Tool Kit (STK) for calculation of debris' station passes and, in particular, of the STK Integration package for interfacing between the main code written in Python and the various AGI routines being available from the graphical user interface otherwise. Moreover, the Collision Analysis

Tool (STK CAT) is used for computations on collision probability and, finally, for orbit determination and propagation the Orbit Determination Tool Kit (ODTK) is used. In contrast to our work in an earlier study [1] where only a single space debris object was tracked by a laser site, the analyses presented in this paper comprise a regime of several thousands of objects making a parallelization of the simulation environment necessary.

As a general outline it shall be noted here that the software generates reference trajectories from a Two-Line-Element (TLE) catalogue for LEO objects. From these trajectories station passes as well as random measurement samples are computed and the orbit determination process is simulated yielding the collision rate and false alert rate of the given network. Afterwards a momentum transfer network can be simulated applying forces induced by laser photon pressure given in target-specific lookup tables from simulations on laser-matter interaction. A second laser tracking simulation based on the modified orbits eventually shows the advantages of the given system in terms of conjunction analysis and avoidance, in particular considering debris vs. debris collisions for which at present collision avoidance manoeuvres are not yet available. In the following, insights on the developed software architecture are given.

The simulation environment is capable of simulating 24/7, twilight and full night laser operation. Since the technical feasibility of blind tracking to space debris has already been demonstrated [4], the analysis focuses on 24/7 operation allowing for larger availability times of each station and in turn smaller network sizes.

3.1 Orbital Data Baseline

As a starting point, a reference trajectory generator (RTG) makes use of catalogued TLE data from USSTRATCOM (U.S. Strategic Command) to compute so-called reference trajectories by a least-squares fit. These trajectories represent the "true" physical position of the respective object in our simulations, irrespective of the fact that for orbit propagation some simplifications are applied in the force model, cf. Tab. 1.

Table 1 Considered forces for the generation of reference trajectories and their numerical implementation.

Force	Numerical Implementation	Ref.
Earth's Gravitational Field	Earth Gravitational Model 1996 (EGM96), degree 20x20	[5]
Atmospheric Drag	NRL-MSISE-00 model	[6]
Solar Radiation Pressure	Objects modelled as a sphere, eclipses taken into account	[7]
Luni-Solar Perturbations	NASA JPL Planetary Ephemerides	[8]

For the sake of simplicity, a drag coefficient of $C_D = 2.2$ and a reflection coefficient of $C_R = 1.0$ have been employed uniformly for all targets.

3.2 Radar Tracking

In order to quantify how a laser tracking network might outperform radar tracking data precision, a radar tracking simulator (RTSim) has been implemented. Due to insufficient knowledge of the location and precision of the USSTRATCOM radar sensors, the simulation of the radar measurement process has been simplified as follows:

- Measurements of all three position components are used instead of range, range rate, azimuth and elevation measurements of a real radar system
- A measurement uncertainty of 10 m in each direction is assumed, following [9]
- For each TLE epoch a single "radar" measurement is generated consisting of three position measurements

Considering the fact that the debris object's physical properties (e.g., mass, area, etc.) are not known exactly, we set slightly deviating values for the drag coefficient ($C_D = 2.0$) and the reflection coefficient of ($C_R = 0.9$). Moreover, we reflect the fact that it is not conceivable to model all contributing force components exactly by choosing a different atmospheric density model for orbit determination, namely Jacchia-Bowman 2008 [10] whereas NRL-MSISE-00 [6] is used in the RTG. These assumptions are applied in the simulation of the LT process as well, in order to get consistent results.

3.3 Collision Alerts

The false alert rate $FAR^{(Radar)}$ is deduced as outlined in Sect. 2 from an extract of CDM data provided from ESA comprising the timespan of Jan 2, 2015 through Oct 7, 2019, which, in particular, covers as well the simulation weeks of our analysis. In those simulation weeks, backwards propagation is carried out for each CDM event yielding the initial state vectors of the conjunction partners at the beginning of the simulation. This allows for an all-on-all conjunction analysis using the reference trajectories which gives the true close approach events. Now close approach warnings from radar tracking are created by removing false positives and adding false negatives considering the false positive and false negative rate from the above-mentioned analysis.

3.4 Laser Tracking

As a prerequisite for laser tracking, station passes are computed for each debris object during the simulation timespan. Passes which take place under local twilight conditions can be flagged in order to assign them the

potential for passive-optical target re-acquisition in case that the maximum permissible position uncertainty for blind tracking has been exceeded due to large measurement gaps, cf. Sect. 4.1.

Temporal gaps between laser tracking measurements can be related to various reasons but not only the geographical station distribution in relation to the orbital parameters. In fact, outage times due to technical failure or maintenance have to be considered as well as laser access constraints due to cloud cover. Therefore, a duty cycle generator is employed which assigns station outage time intervals of one hour each using a uniform random distribution. Per default, a duty cycle of $DC = 50\%$ is employed in the majority of our simulations. Beyond this, the impact of DC on the network performance parameters is analysed and, moreover, a station-specific duty cycle is assigned on the basis of cloud cover statistics in advanced simulations, cf. Sect. 4.3. and 6.3.

Facing the multitude of space debris objects to be tracked, prioritization is needed in case that several objects pass a ground station in the same time interval to derive a schedule of laser ranging measurements. In the first step of this scheduling algorithm, the first tracklet of each object during the simulation timespan is selected. In case of a scheduling conflict, prioritizing of debris objects is undertaken then with respect to (in descending order) a) the debris' involvement in a conjunction event, b) the urgency of its measurement in terms of the remaining time to TCA if a) applies, c) the urgency of its measurement in terms of the remaining time to laser tracking data expiry, cf. Sect. 4.1. Moreover, if tracking data of a target has already expired, its ranging measurement is postponed to its soonest tracklet during station twilight for object re-acquisition, cf. Sect. 4.2. Note that in the analysis of the laser catalogue scenario re-acquisition is not considered a viable option but data expiry would constitute loss of the respective object. Moreover, prioritization criteria a) and b) are discarded in that scenario since its analysis focuses on laser catalogue capacity solely.

Once a target is scheduled, its laser ranging measurements during a station pass are represented by assignment of randomized range data to the trajectory based on a Gaussian $N(\mu, \sigma^2)$ distribution where μ denotes the true range and σ is the laser ranging accuracy, which has been set to $\sigma = 1.5\,m$. The laser measurements are simulated with a sampling rate of 1 min^{-1}.

For orbit determination (OD) on the basis of laser tracking data, the simulation time interval is evenly split into orbit determination intervals Δt_{OD} of 9 hours each. Starting with an initial estimate of the object's state vector and covariance matrix, ODTK's Kalman filter is used for processing of laser measurements in the respective OD interval. From the end of that interval, the new orbital estimate and its covariance matrix is propagated to the end of the simulation interval for a conjunction analysis on the propagated ephemeris which yields the close approach warnings that would be generated from laser tracking. Subsequently, this process is repeated for the adjacent OD interval until to the end of the simulation time.

3.5 Conjunction Analysis

To address the large number of debris objects in an all-on-all conjunction analysis, pre-filtering of the objects on TLE basis has been implemented. For this purpose, a Least Squares Fit on ephemeris data is undertaken which yields the TLE data. The respective conjunction pairs are filtered then with respect to apogee/perigee, orbit path, time, and range, which excludes a large number of them from the subsequent exhaustive analysis of target ephemeris vs. chaser ephemeris using the AdvCat tool of STK CAT. AdvCat operation is configured here for the usage of Alfano's algorithm outlined in [11].

3.6 Momentum Transfer

Laser-induced forces from photon pressure have been computed in Monte Carlo simulations with DLR's code Expedit. The code allows for the computation of laser-induced momentum and heat to arbitrarily shaped targets and is described in [12]. Originally designed for pulsed laser irradiation yielding laser ablation, Expedit has been adapted here for computation of laser-induced photon pressure. In the related simulations the target's shape, size, and its random orientation within the MT laser beam are accounted for. Moreover, pointing uncertainty is considered as well as, atmospheric beam attenuation, turbulence, and its compensation to a realistic degree by adaptive optics. A detailed report on the simulations and the related feasibility analyses is intended for later publication [13].

Within the network simulations presented here, however, the resulting data is interfaced to the simulation environment via target-specific lookup tables giving magnitude and scatter of laser forces as a function of the irradiation's zenith angle. If MT laser operation is assigned to a debris' station pass, laser-induced force $F(\zeta)$ in direction of laser beam propagation is computed if the zenith angle is within the MT laser irradiation interval, i.e., $\zeta \in [15°; 65°]$ *and* the pass segment matches the MT laser irradiation strategy (see below). In turn, the velocity increment $\Delta v = F(\zeta) \cdot \Delta t_{MT}/m$ is applied to the debris' trajectory by an instantaneous orbit modification maneuver. Here, m denotes the object's mass and $\Delta t_{MT} = 5\,s$ gives the discretization timestep of the MT station pass simulation.

Since the applied forces from laser photon pressure are in the micronewton range, the altitude gain from acceleration is neglectable and, thus, both deceleration

and acceleration of the target are viable options. This leads to the question which of those two options to choose. In case of a debris vs debris conjunction we are even faced with four possibilities to choose from for each close approach event. However, it's obviously not reasonable to first accelerate an object and then decelerate it or vice versa. Hence, the irradiation strategy has to be derived per object and not per event. Therefore, the most critical event is selected for each object (the "decision event") and all options are simulated for this event. A postprocessing algorithm now finds for each decision event the optimal solution and assigns the corresponding irradiation strategy to the object. Finally, a last simulation is carried out using the optimized irradiation strategy.

4 CONSTRAINTS

4.1 Tracking Data Expiry

Each tracking measurement is associated with a measurement precision, which yields a decrease in position and velocity uncertainty of the measured object. In this regard, orbit propagation subsequent to a tracking measurement not only means propagation of the object's trajectory but as well error propagation of the orbit state. Obviously, covariance increases over time which makes the measured data less useful and constitutes a demand for an update of orbital data by another tracking measurement. Furthermore, due to the aforementioned covariance increase laser blind tracking is limited by the acceptable a-priori uncertainty for a new tracking measurement. In case this a-priori uncertainty is exceeded, the narrow laser cone is more likely to miss the target and will be unsuccessful in receiving photon returns from the object, which would be needed to establish a closed loop for permanent laser ranging during the scheduled timeframe for measurement.

For blind tracking the maximum tolerable timespan without a ranging measurement depends on the divergence of the tracking laser beam, the initial elevation for target tracking, and the altitude of the debris object. The maximum along-track uncertainty that allows blind tracking is derived using the beam-target hit probability model. The model assumes, that the target is spherically-shaped and photon returns can be measured as long as the target diameter intersects with the beam diameter d_{beam}. The latter is computed by small-angle approximation as

$$d_{beam} = 2 * \alpha_{Div} * z \qquad (5),$$

where α_{Div} is the beam divergence angle and z is the target distance. Compensation by tracking software, spiral search methods, etc. is not considered. A linear beam divergence of 30 arcsecs is assumed together with constant orbit uncertainty in the local orbital frame (radial (r), in-track (i), cross-track (c)), which is dominated by the along-track uncertainty. On top of that, a simple pass geometry model is used, for which we derived a probability distribution, i.e., the likelihood of a pass having a specific geometry. This distribution is used for the Monte Carlo simulations together with the hit probability model. Based on that, the maximum along-track uncertainty is found as shown in Fig. 1. Limitations related to returning signal energy, however, are neglected in these considerations.

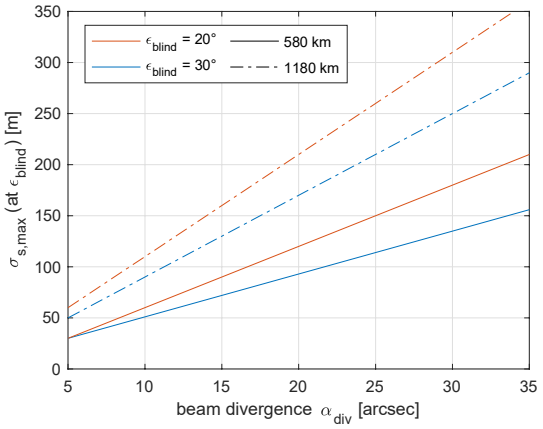

Figure 1. Maximum along-track uncertainty $\sigma_{s,max}$ for a required hit probability of 80% in at least 80% of the randomly sampled passes and for different tracking elevations and object altitudes (circular orbits assumed).

To derive an empirical formula for the expiry time of laser tracking data, the covariance evolution has been analysed using laser tracking simulation results. For each object the temporal course of the along-track covariance of its position was recorded for the entire simulation timespan. From this data, the 10 longest timespans without laser measurements have been aggregated for every debris object. Subsequently, a linear fit has been applied to derive the slope of covariance which finally yields the time that passes after a laser tracking measurement, before the maximum along-track covariance is reached at which a target can be re-acquired in 24/7 blind tracking.

The results for laser tracking data expiry is shown in Fig. 2. For the network simulations of the laser catalogue scenario, the quadratic fitting function shown in red is mainly used, which approximately represents the median of the data, supplemented by a few simulations using the function indicated in blue representing the 90-percentile of the data.

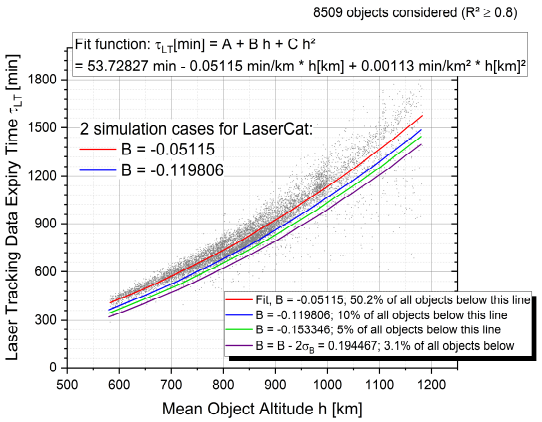

Figure 2. Expiry time of laser tracking data w.r.t. the maximum in-track uncertainty permissible for 24/7 "blind" tracking, i.e., without any means for target re-acquisition.

4.2 Target Re-Acquisition

For re-acquisition of an object whose position uncertainty has grown too large for "blind" laser tracking, passive-optical methods have to be used which demand for twilight conditions. The time span available for target re-acquisition, however, strongly depends from the observation site geographic latitude, cf. Fig. 3, as well as from the time of the year.

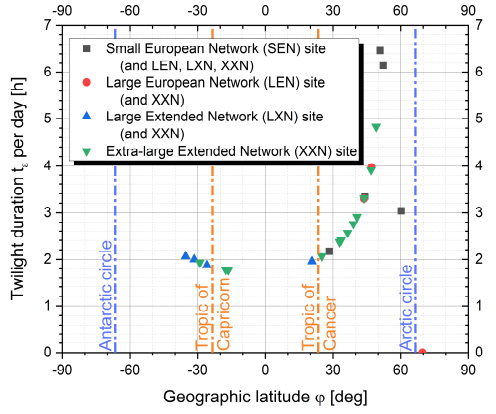

Figure 3. Mean twilight duration per day calculated from [13] for the employed network stations in the simulation timespan of July 12 – 18, 2019. Durations refer to the time interval of nautical and astronomical twilight as a coarse estimate of fortunate conditions for passive-optical detection.

4.3 Cloud Cover

The site-specific cloud coverage has to a great extent been derived in an earlier study [1] from the ERA-Interim database of the European Center for Medium-Range Weather Forecast (ECMWF) which comprises an exhaustive dataset of a large variety of weather data products. For the scope of laser ranging, global data on total cloud cover CF on a 3-hourly basis through the 11-year timeframe of 2007-2017 has been employed with a spatial resolution of a 0.75° grid (geographical latitude and longitude, respectively) with subsequent spatial interpolation for the site geographical coordinates.

Based on the statistical analysis on cloud coverage and laser tracking observations shown in [1] we use an empirical threshold of $CF_{th} = 50\%$ maximum cloud cover for laser tracking. Hence, we define the station-specific laser access rate p_{CF} as the fraction of time intervals for which the mean cloud cover is below this threshold, $\langle CF \rangle < CF_{th}$ which, based on the large timeframe covering an entire solar cycle, gives a fair proxy for laser site ranking in terms of access to space, cf. Fig. 4.

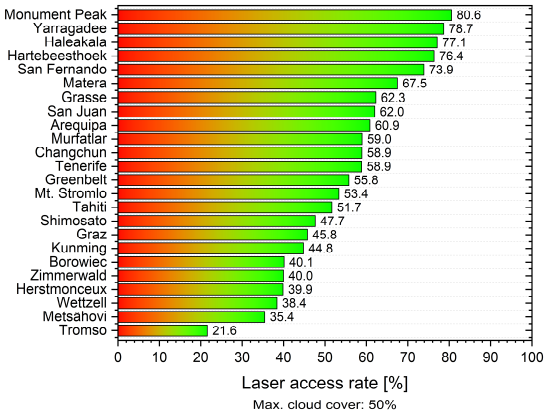

Figure 4. Laser access rate for network sites based on ECMWF data on cloud fraction for 2007-17.

4.4 Atmospheric Beam Attenuation

Like cloud coverage, station data on atmospheric attenuation had mostly been derived for the work described in [1] from ECMWF resources, however, from the Near-real time archive of the Copernicus Atmosphere Monitoring Service (CAMS) as well as of its respective Monitoring Atmospheric Composition and Climate - Interim Implementation (MACC-II). Using ECMWF data and forecast values for aerosol optical depth (AOD) at wavelengths of $\lambda = 865\ nm$ and $\lambda = 1240\ nm$, the respective value of $AOD_{\lambda=1064\ nm}$ has been interpolated using the Angstrøm coefficient.

Unlike cloud coverage, AOD data has not been used for LT but only for MT simulations. It serves to modify the tabulated data for the laser-induced force F_{ref}, calculated with a reference aerosol optical depth of $AOD_{ref} = 0.144$, accordingly matching the site-specific AOD value as well as the zenith angle ζ of MT laser irradiation employing

$$F = F_{ref} \cdot \exp\left[\left(AOD_{ref} - AOD\right) \cdot \sec\zeta\right] \quad (6).$$

Again, a station ranking can be undertaken here considering now the mean AOD value for each site, cf. Fig. 5.

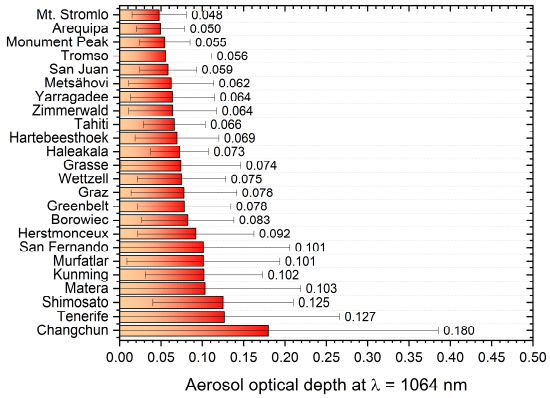

Figure 5. Site ranking considering atmospheric beam attenuation at $\lambda = 1064\ nm$ for network sites based on CAMS data on aerosol optical depth for 2007-17.

4.5 Site Location and Orbit Parameters

To assess the suitability of a given MT site location with respect to the orbital parameters of the considered objects, the average Δv -potential $p_{\Delta v}$ is defined as follows:

$$p_{\Delta v} = \frac{1}{N}\sum_i \int \Delta v_{\text{along}}(\epsilon_{\max}, OE_i) \cdot \nu(\phi, OE_i) \cdot p(\epsilon_{\max}, \phi, OE_i) d\epsilon_{\max}, \quad (7)$$

N is the number of considered objects, Δv_{along} is the along-track Δv as a function of pass geometry that is parametrized by the maximum reached elevation $\epsilon_{\max}$, ν is the long-term mean station revisit frequency, ϕ is the geographic latitude of the station, OE_i are the orbital elements of object i, and p is the probability that a pass will reach an elevation $\epsilon_{\max}$,

As an indicator for suitable MT station latitudes, the normalized Δv potential $p_{\Delta v}$ averaged over all considered objects (see Section 5.1) is shown by Fig. 6 as a function of station latitude ϕ. The simplified analytical model presented by [15] is used to approximate ν and p. Clearly, high latitudes around $\phi = 80$ deg are preferable in this regard. This is due to the fact that many objects are in highly inclined orbits, where high-elevation passes, which entail large achievable along-track Δv values, and high station revisit frequencies are combined.

From these findings and the results on weather data analysis (see Section 4.3) a station ranking has been derived, cf. Tab. 2.

Table 2. Station ranking derived from cloud-related laser access p_{CF} and potential $p_{\Delta v}$ for momentum transfer as computed from the site's geographical latitude φ.

Site name	φ [°]	p_{CF} [%]	$p_{\Delta v}$ [-]	Station Ranking [-]
San Fernando	36.47	73.9	0.0096	0.0071
Matera	40.65	67.5	0.0098	0.0066
Grasse	43.75	62.3	0.0105	0.0066
Murfatlar	44.14	59	0.0105	0.0062
Changchun	43.79	58.9	0.0105	0.0062
Monument Peak	32.89	80.6	0.0076	0.0061
Hartebeesthoek	-25.89	76.4	0.0078	0.0059
Yarragadee	-29.05	78.7	0.0072	0.0056
Metsähovi	60.22	35.4	0.0148	0.0053
Haleakala	20.71	77.1	0.0064	0.0049
Tromsø	69.66	21.6	0.0225	0.0049
Greenbelt	39.02	55.8	0.0085	0.0048
Mt. Stromlo	-35.32	53.4	0.0084	0.0045
San Juan	-31.51	62	0.0071	0.0044
Tenerife	28.30	58.9	0.0073	0.0043
Herstmonceux	50.87	39.9	0.0103	0.0041
Arequipa	-16.47	60.9	0.0063	0.0038
Graz	47.07	45.8	0.0083	0.0038
Borowiec	52.28	40.1	0.0088	0.0035
Shimosato	33.58	47.7	0.0072	0.0034
Kunming	25.03	44.8	0.0074	0.0033
Zimmerwald	46.88	40	0.0083	0.0033
Tahiti	-17.58	51.7	0.0064	0.0033
Wettzell	49.14	38.4	0.0084	0.0032

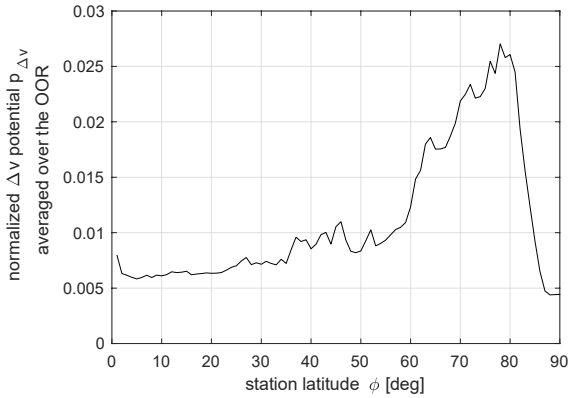

Figure 6. Normalized along-track Δv potential $p_{\Delta v}$ averaged over all considered objects.

5 SIMULATION SETUP

5.1 Operational Orbital Regime

The Operational Orbital Regime (OOR) of this work is given by the orbital parameter constraints of

- semi-major axis $a \in [6950\ km; 7550\ km]$,
- numerical eccentricity $e \in [0; 0.2]$, and
- inclination $i \in [65°; 110°]$.

A snapshot of the USSTRATCOM catalogue as of 2 July 2019 has been filtered with respect to the above-mentioned constraints yielding overall 10916 objects. 1077 of them have been identified using Celestrak data as active satellites and, therefore, have been flagged in the simulations as not suitable as targets for MT laser irradiation. For overall 1467 integer objects – payloads, rocket bodies and mission-related objects – their mass, size and shape has been derived from an extract of the Database and Information System Characterising Objects in Space (DISCOS) [16] provided by the European Space Operation Centre (ESOC). For fragmentation debris (7634 catalogued OOR objects), the debris population from the Meteoroid and Space Debris Terrestrial Environment Reference (MASTER) model was employed to derive statistically founded estimates for the cross-sectional area and mass of each debris target in agreement with radar cross-sections from DISCOS. As a remainder, 738 debris objects have been discarded, mostly due to missing information on mass or on optical cross-sectional area which is required for appropriate laser force computation, cf. Sect. 3.6.

5.2 Laser Station Networks

The simulations cover four different network configurations (cf. Fig. 7 and Fig. 8):

- The small European network (SEN) consists of 5 stations and is solely based in Europe.
- The large European network (LEN) adds three European sites to the SEN.
- The large extended network (LXN) adds four non-European sites to the SEN.
- The extra-large extended network (XXN) comprises of 24 internationally distributed sites including those of the SEN, LEN and LXN.

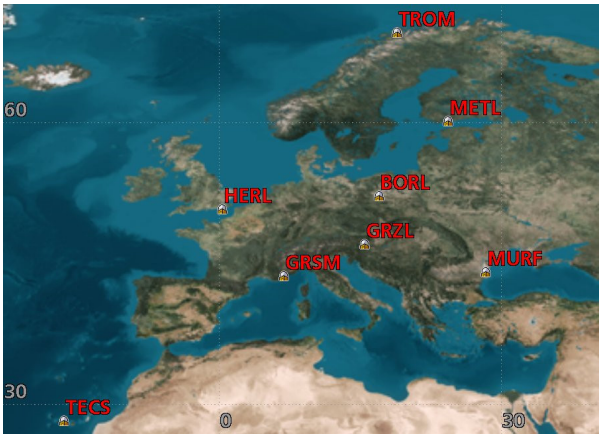

Figure 7. Map of the large European laser station network (LEN).

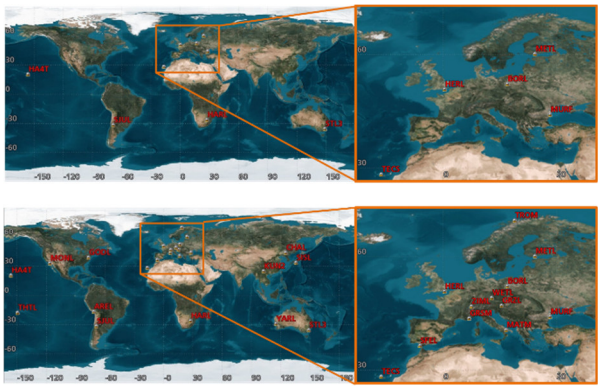

Figure 8. Map of the large extended (LXN, upper) and extra-large extended (XXN, lower) laser station network. The small European network (SEN), which is part of LXN, is shown in the upper right.

5.3 Simulation Time Interval

In the following the results for two simulation time frames, each lasting one week, will be discussed, cf. Tab. 3.

Table 3. Simulation time frames. Each simulation starts and stops at the indicated dates at 00:00:00 UTC.

Week	Simulation Start	Simulation Stop
A	12.07.2019	19.07.2019
B	01.09.2019	08.09.2019

A uniform duty cycle of 35% and 50% as well as the site-specific duty cycle, based on the weather analysis outlined in section 4.3, have been analysed.

6 RESULTS AND DISCUSSION

6.1 Laser-based CDM Verification

For the analysis of laser tracking in response to conjunction alerts, i.e., on demand tracking, five duty cycle samples have been created for each simulation week and duty cycle value. Fig. 9 shows the dependency between collision rate (CR) and network size for simulation week A and B, respectively.

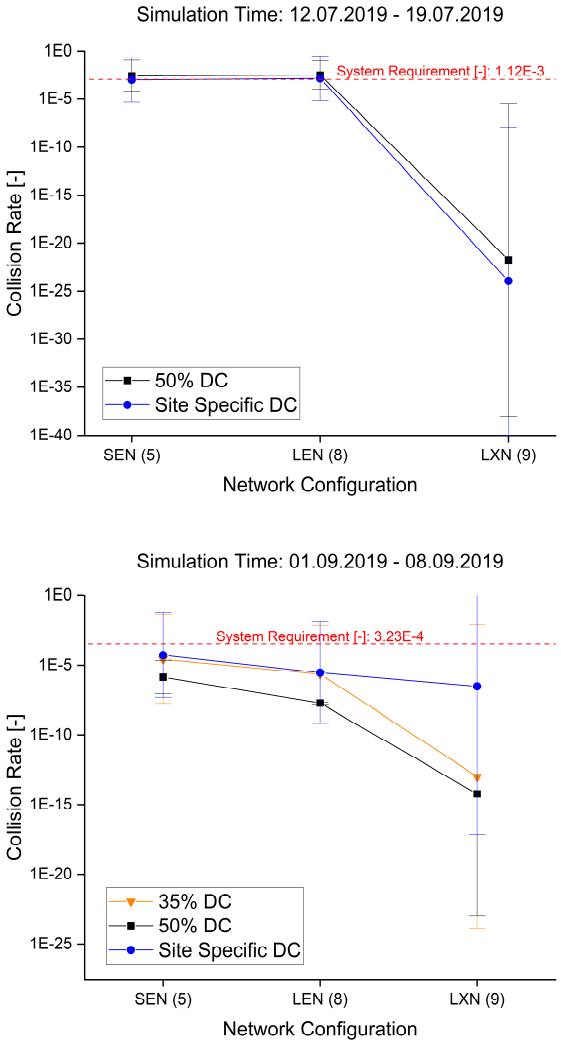

Figure 9. Dependency between collision rate and network size for simulation week A (upper graph) and B (lower graph).

While the system requirement, which is a reduction of the CR by 95% with respect to the radar system, is achieved by each network configuration in simulation week B, this is only the case for the LXN configuration in simulation week A. Furthermore, one can see that the global network configuration generally outperforms the European configurations.

Regarding the FAR it has been shown, that the system requirement, i.e., a reduction of the FAR by one order of magnitude, is fulfilled by each network size for both simulation weeks. However, no relationship between FAR and network size or duty cycle value could be found, cf. Fig. 10.

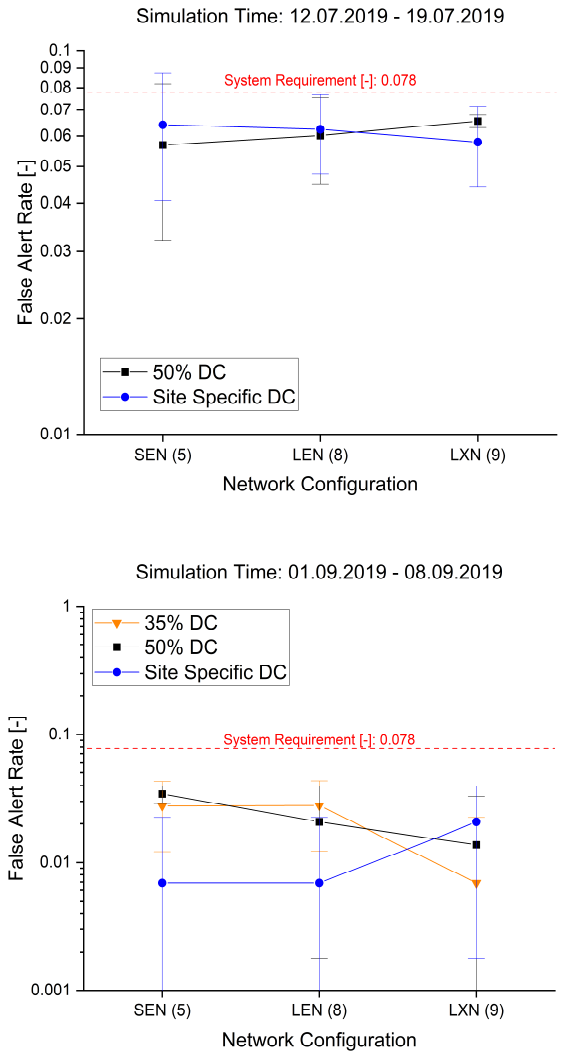

Figure 10. Dependency between false alert rate and network size for simulation week A (upper graph) and B (lower graph).

In sum, the LXN as the recommended option for an on-demand laser tracking network can be characterized by the following mean parameters:

- Number of tracklets per object within one week timespan: 67
- Number of tracklets per day: 1345
- Average tracklet duration: 4.8 min
- Achievable a-priori position accuracy for the next station pass:
  $\sigma_r = 31.9\ m, \sigma_i = 114.4\ m, \sigma_c = 78.1\ m$
- Position covariance size directly after laser measurement:
  $\sigma_r = 11.5\ m, \sigma_i = 21.8\ m, \sigma_c = 24.8\ m$
- Typical position covariance size averaged over one week:
  $\sigma_r = 59.5\ m, \sigma_i = 207.2\ m, \sigma_c = 149.2\ m$

6.2 Laser Tracking Network Capacity

In order to perform the laser catalogue capacity analysis, 10 duty cycle samples have been created for each network configuration and duty cycle value. As shown in Fig. 11 the dependency on the chosen simulation week is neglectable (the deviation is between 0.03% and 3.62%) and, thus, the results of both simulation weeks have been combined yielding 20 samples for each data point.

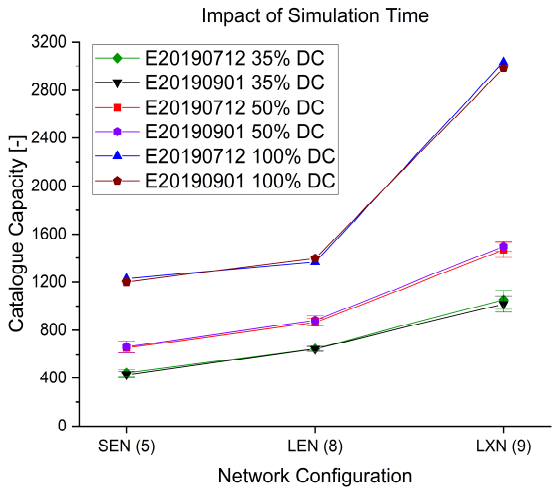

Figure 11. Impact of simulation time on the results for the catalogue capacity of the analysed laser tracking networks.

The dependency between catalogue capacity and duty cycle value is shown in Fig. 12. For the LXN a 100% duty cycle value yields a maximum catalogue capacity of 3007 objects, while a 35% duty cycle value reduces the catalogue capacity to 1035 objects. Interestingly, the LXN performs better going from 50% duty cycle to site-specific duty cycle, while the SEN and LEN perform worse in this case. This is due to the fact that the additional stations in the LXN achieve site-specific access rates larger than 50%, while the LEN and the SEN have a mean site-specific access rate of 41.5% and 44.6%, respectively (mean value weighted by the total number of passes).

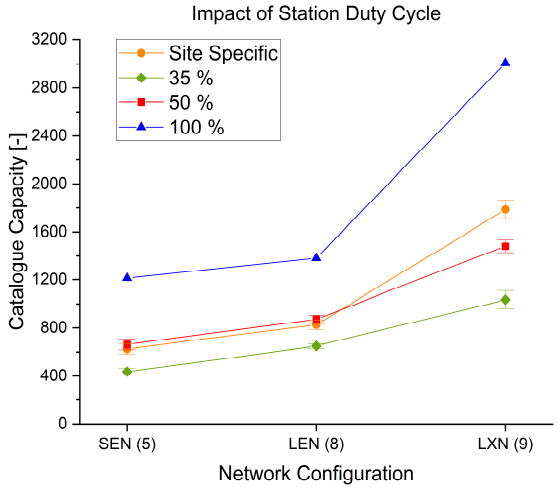

Figure 12. Impact of station duty cycle on the results for the catalogue capacity of the analysed laser tracking networks.

In order to see whether a 24-station network is capable of tracking all 9101 OOR objects, a 100% duty cycle simulation has been carried out for simulation week A with the XXN network using the red curve for expiry time vs. altitude (cf. Fig. 2). Furthermore, a 10-station network comprising of all LXN stations and San Fernando (SFEL) has been analysed using the same setup. As shown in Fig. 13 the catalogue capacity is limited to 5448 objects even with the 24-station network. The discontinuous growth from LEN to LXN is due to the fact that the LXN has a global coverage in contrast to the LEN and, thus, continuous tracking is alleviated.

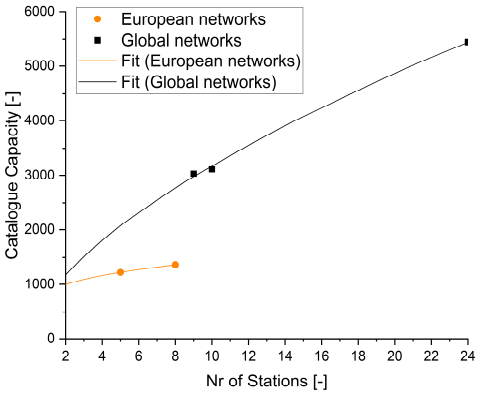

Figure 13. Impact of number of stations on the results for the catalogue capacity of the analysed laser tracking networks.

Both for the European network configurations as well as for the international sites, an exponential function

$$n_{Objects_{Laser\,Cat}} = a * n_{Stations}^{b} \qquad (8)$$

has been fitted to the data, where $n_{Stations}$ denotes the number of laser tracking stations and $n_{Objects_{Laser\,Cat}}$ is the laser catalogue capacity. Tab. 4 shows the fitting parameters for both cases.

Solving now for 9101 OOR objects yields a network size of 54 stations for an internationally distributed network and an unrealistic duty cycle of 100%. If the sites are restricted to Europe, the number increases significantly to 30505. The previous analysis has shown a nearly linear relationship between duty cycle and catalogue capacity for an international network configuration. Thus, 108 stations would be required assuming a more realistic duty cycle of 50%.

Table 4. Fitting parameters a and b for exponential fit of catalogue capacity vs. number of stations.

Network Configuration	a [-]	b[-]
European	847	0.23
Global	769	0.62

6.3 Collision Avoidance by Photon Pressure

In order to analyse the performance of a combined LTMT system, the following simulation configuration has been chosen:

- Min. debris elevation for LT: $\epsilon = 15°$,
- Min. LT measurement time: $\Delta t_{LT} = 60\ s$,
- Laser ranging accuracy: $\beta_{LR} = 0\ m$,
- Laser ranging precision: $\sigma = 1.5\ m$,
- LT accuracy: $\sigma_t = 0.1"$,
- MT laser power: $P_L = 40\ kW$,
- Min. debris elevation for MT: $\epsilon = 25°$,
- Max. sun elevation for re-acquisition: $\epsilon = -6°$,
- Single duty cycle sample (site-specific),
- Red curve for expiry time vs. altitude (cf. Fig. 2).

The first analysis shall serve as a baseline for the subsequent network optimization and covers the four standard network configurations (see Section 5.2), while each site is treated as a LTMT site, i.e., they have both capabilities. As shown in Fig. 14 only the XXN achieves a reduction of the CR below 5% of the CR value without MT and, thus, fulfils the system requirement (SR). Hence, the network optimization is carried out between the LXN and the XXN.

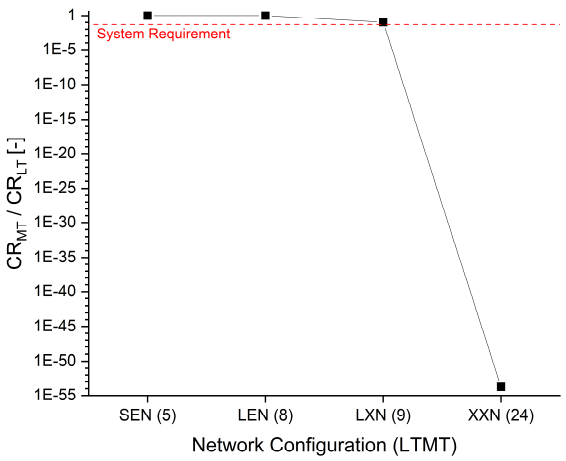

Figure 14. Fraction of collision rate with MT and without MT vs. network configuration. The number of stations is given in brackets.

Now, MT sites have been removed from the XXN network using a bisectional approach and following the station ranking from Tab. 2, while the LT network has been left unchanged in the XXN configuration. Fig. 15 shows the ratio of the CR with MT and the CR without MT vs number of MT stations for this analysis. Even for the configuration LXN + San Fernando (SFEL), which is 10 MT sites, the SR is surpassed by 20 orders of magnitude. Thus, the decision has been made to analyse 6 MT stations, which is actually an optimization between SEN and XXN. This configuration is 10 orders of magnitude below the SR. Even for one single MT station, the SR is still surpassed by three orders of magnitude.

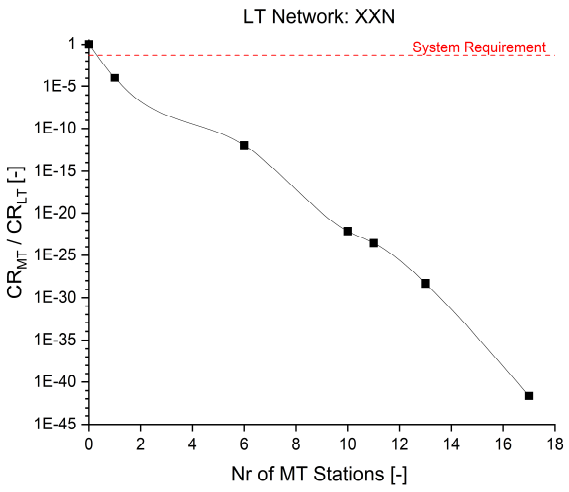

Figure 15. Ratio of the collision rate with MT and without MT vs. number of MT stations. LT is performed using the XXN network. A spline curve has been used to connect the data points.

However, since the costs for this configuration are higher than the costs of 12 LTMT stations, in a subsequent analysis LTMT sites are added to the LXN network following the station ranking (cf. Tab. 2) until the SR is met. The outcome of this analysis is depicted in Fig. 16. The SR is met with 10 LTMT stations yielding a CR reduction of 4.7%.

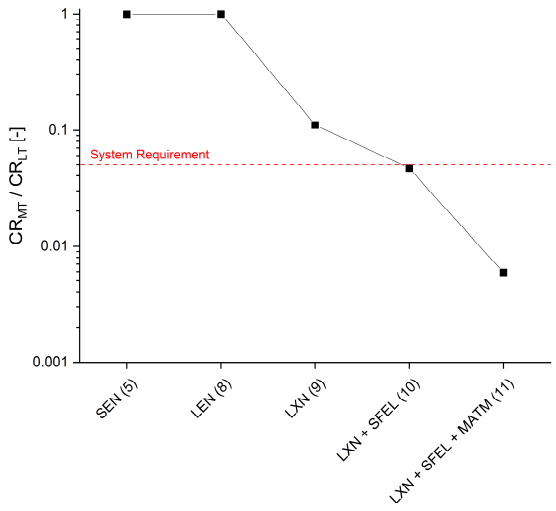

Figure 16. Ratio of the collision rate with MT and without MT vs. LTMT network configuration. Each site has both capabilities (LT and MT).

Hence, in a final step the size of the MT network is reduced further, while keeping the LT network unchanged in the configuration LXN + SFEL. The final analysis now shows, that if the worst performing station according to Tab. 2 (Borowiec) is changed from LTMT to LT, we get a CR reduction of 93% and, thus, the SR is not fulfilled anymore. Therefore, the optimization is completed and the final network layout is LXN + SFEL, whereas all stations are LTMT sites.

7 SUMMARY AND OUTLOOK

A simulation environment has been developed, which simulates a LTMT network and assesses its performance in terms of CR and FAR. Station specific weather data as well as object specific laser forces from LMI simulations have been used to keep the simulations as realistic as possible. Two operational scenarios have been analysed: A laser catalogue scenario, where all 9101 objects of the OOR are tracked, and an on-demand scenario, which focuses on objects with close approach warning. The simulations have shown, that 9 laser tracking stations are sufficient to reduce the CR by 95% and the FAR by a factor of 10 with respect to the radar system. A network of 10 LTMT stations is capable of reducing the CR even further down to 95% of the value without MT. In order to continuously track all 9101 OOR objects a network with more than 24 Stations is required. A global network configuration has shown a distinctly better performance than an equally sized European network and, thus, is the recommend option. For future LTMT networks a trade-off between costs and network performance has to be made, where the key design parameter could be the envisaged size of the laser catalogue.

Possible topics for future research include for example a comparison of laser-ablative (single pulse and/or repetitive) with photon pressure methods, an analysis of a hybrid network consisting of radar and laser stations or the addition of space-based sensors to the simulations. Furthermore, the computation of collision rate and false alert rate in a laser catalogue scenario as well as the comparison of 24/7 tracking and twilight or full night tracking operation could be investigated in the future. Finally, more sophisticated algorithms for scheduling and for the optimization of the momentum transfer strategy might be implemented.

Beyond technological challenges on the way towards a possible implementation of a future LT or LTMT network, aspects of laser safety, operational safety as well as legal issues have to be addressed properly, which is, e.g., reflected in a more general paper submitted by our group for this conference [17].

8 ACKNOWLEDGMENTS

The authors thankfully acknowledge funding of our study LARAMOTIONS (SSA P3-SST-XV) by ESA under grant no. 4000127148/19/D/CT within the Space Surveillance and Tracking segment of ESA's Space Situational Awareness programme.

Moreover, the sound and inspiring discussions with the other colleagues of our study team are greatly appreciated giving a big thankyou to Gerd Wagner (DLR), Paul Wagner (DLR), Ewan Schafer (DLR), Jürgen Kästel (DLR), Urs Hugentobler (TUM), Tomasz Suchodolski (CBK-PAN), Pawel Lejba (CBK-PAN), Egon Döberl (ASA), Dietmar Weinzinger (ASA), Wolfgang Promper (ASA).

Furthermore, the access to the USSTRATCOM catalogue of TLE data, the ESA DISCOS database as well as ESA's MASTER-8 debris population model is thankfully appreciated.

Finally, the access to weather data from ERA-Interim, CAMS Near-realtime archive and MACC-II as of 2018 through the ECMWF is greatly acknowledged. As a disclaimer it has to be noted that neither the European Commission nor ECMWF is responsible for the any use the downloaded weather data.

9 REFERENCES

1. Phipps, C. et al. (2012). Removing orbital debris with lasers, *Adv. Space Res.* **49**, 1283-1300.
2. Yang Yang, F. et al. (2016). Light Force photon-pressure collision avoidance: Efficiency analysis in the current debris environment and long-term simulation perspective, *Acta Astronaut.* **126**, 411-423.
3. Alfano, S. & Oltrogge, D. (2018). Probability of Collision: Valuation, variability, visualization, and validity, *Acta Astronaut.* **148**, 301-316.
4. Lejba, P. et al. (2018). First laser measurements to space debris in Poland, *Adv. Space Res.* **61**, 2609-2616.
5. Lemoine, F. et al. (1997). The development of the NASA GSFC and NIMA joint geopotential model, *Gravity, Geoid and Marine Geodesy* **117**, 461–469.
6. Picone, J. et al. (2002). NRLMSISE-00 empirical model of the atmosphere: Statistical comparisons and scientific issues, *Journal of Geophysical Research Atmospheres* **107**.
7. Vallado, D.A. (2013). Fundamentals of Astrodynamics and Applications, , 4th edition, Microcosm Press, New York, USA.
8. Folkner, W. et al. (2014). The Planetary and Lunar Ephemerides DE430 and DE431, IPN Progress Report, Online at ftp://naif.jpl.nasa.gov/pub/naif/generic_kernels/spk/planets/de430_and_de431.pdf (as of 19 Mar 2021)
9. Kirschner, M. et al. (2012). Orbit Precision Analysis of Small Man-Made Space Objects in LEO Based on Radar Tracking Measurements, In *23rd International Symposium on Space Flight Dynamics*, Pasadena, CA, USA.
10. Bowman, B. et al. (2008). A New Empirical Thermospheric Density Model JB2008 Using New Solar and Geomagnetic Indices, *AIAA Paper* 2008-6438, doi: 10.2514/6.2008-6438.
11. Alfano, S. (2005). A Numerical Implementation of Spherical Object Collision Probability, *J. Astronaut. Sci.* **53**, 103-109.
12. Scharring, S. et al. (2018). Momentum predictability and heat accumulation in laser-based space debris removal, *Opt. Eng.* **58**(1), 011004, doi: 10.1117/1.OE.58.1.011004.
13. Scharring, S. et al. Review on Numerical Simulations on Laser-matter Interaction with Debris Objects in the low Earth orbit. In preparation for journal submission.
14. Wolfram Data Repository, Online at https://datarepository.wolframcloud.com/ (as of 4 Nov 2020).
15. Bamann, C. et al. (2020). Analysis of collision avoidance via ground-based laser momentum transfer, *J. Space Safety Engineering* **7**, 312-317.
16. Database and Information System Characterising Objects in Space (DISCOS), European Space Operations Centre (ESOC) of the European Space Agency (ESA), Online at https://discosweb.esoc.esa.int/ (as of 12 March 2021)
17. Scharring, S. et al. (2021). Potential of using ground-based high-power lasers to decelerate the evolution of space debris in LEO. Submitted for this conference.